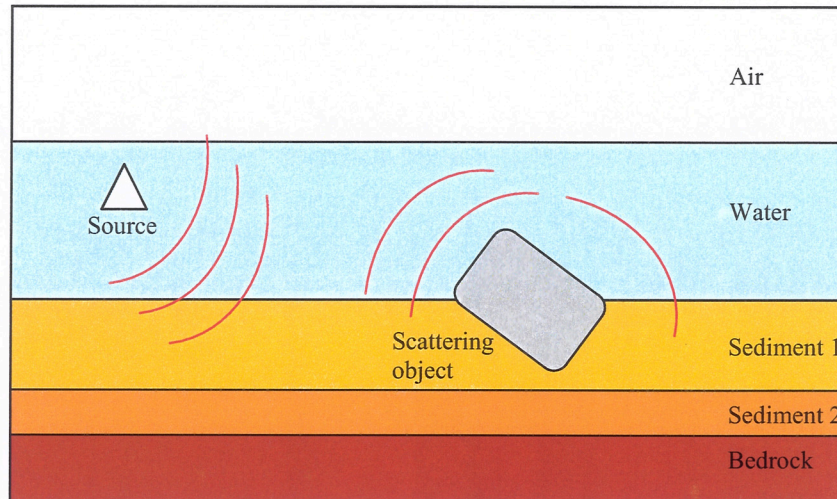


Anders Ellgardt

# Electromagnetic scattering from smooth objects across layer interfaces



SWEDISH DEFENCE RESEARCH AGENCY

Systems Technology  
SE-172 90 Stockholm

FOI-R--1162--SE

January 2004

ISSN 1650-1942

**Technical report**

Anders Ellgardt

# Electromagnetic scattering from smooth objects across layer interfaces

<b>Issuing organization</b> FOI – Swedish Defence Research Agency Systems Technology SE-172 90 Stockholm	<b>Report number, ISRN</b> FOI-R--1162--SE	<b>Report type</b> Technical report
	<b>Research area code</b> 4. C4ISR	
	<b>Month year</b> January 2004	<b>Project no.</b> E6706
	<b>Customers code</b> 5. Commissioned Research	
	<b>Sub area code</b> 43 Underwater Sensors	
	<b>Author/s (editor/s)</b> Anders Ellgardt	
<b>Project manager</b> Peter Krylstedt		
<b>Approved by</b> Monica Dahlén		
<b>Sponsoring agency</b> FMV		
<b>Scientifically and technically responsible</b> Johan Mattsson		
<b>Report title</b> Electromagnetic scattering from smooth objects across layer interfaces		
<b>Abstract (not more than 200 words)</b> <p>In this report the theory and a program for computing electromagnetic ELF scattering from a smooth perfectly conducting object positioned across layer interfaces in a stratified environment is presented. The program uses a boundary element method to compute the current density on the scatterer and the fields outside the scattering object. To be able to position the scatterer in multiple layers the mesh is refined so that no face in the mesh is positioned in more than one layer. The alteration of the mesh is done through division of the faces positioned in more than one layer. To increase the speed of the program an approximation of the dyadic Green's function within a face is presented which decreases computational time of the collocation integral with a factor of six. The results and convergence of the program are compared with a program based on a global Galerkin's method for the case when the scatterer is positioned in one layer. Two numerical examples are presented in the end of the report.</p>		
<b>Keywords</b> electromagnetic, scattering, stratified media, dyadic Green's functions, dispersive media		
<b>Further bibliographic information</b>	<b>Language</b> English	
<b>ISSN</b> 1650-1942	<b>Pages</b> 24 p.	
<b>Price acc. to pricelist</b>		

<b>Utgivare</b> Totalförsvarets Forskningsinstitut - FOI Systemteknik 172 90 Stockholm	<b>Rapportnummer, ISRN</b> FOI-R--1162--SE	<b>Klassificering</b> Teknisk rapport
	<b>Forskningsområde</b> 4. Spaning och ledning	
	<b>Månad, år</b> Januari 2004	<b>Projektnummer</b> E6706
	<b>Verksamhetsgren</b> 5. Uppdragsfinansierad verksamhet	
	<b>Delområde</b> 43 Undervattenssensorer	
<b>Författare/redaktör</b> Anders Ellgardt	<b>Projektledare</b> Peter Krylstedt	
	<b>Godkänd av</b> Monica Dahlén	
	<b>Uppdragsgivare/kundbeteckning</b> FMV	
	<b>Tekniskt och/eller vetenskapligt ansvarig</b> Johan Mattsson	
<b>Rapportens titel (i översättning)</b> Elektromagnetisk spridning från glatta objekt som skär gränssytor		
<b>Sammanfattning (högst 200 ord)</b> <p>I denna rapport presenteras teorin och ett program för att beräkna spridning från glatta perfekt ledande objekt som skär gränssytor i en skiktad miljö. Programmet använder sig av en randelementmetod för att beräkna ytströmtätheten på spridarens yta och fälten utanför det spridande objektet. För att kunna placera spridaren i fler än ett skikt så måste ytans rutnät manipuleras så att en yta i rutnätet endast befinner sig i ett skikt. Manipulationen sker genom att man delar på ytor i rutnätet som är positionerade i mer än ett skikt. För att förkorta programmets beräkningstid så används en approximation av de dyadiska greensfunktionerna inom en yta så att beräkningstiden av kollokationsintegralen minskas med en faktor sex. Resultat och konvergens av programmet jämfördes mot ett program som använder sig av en global Galerkin metod för fallet då spridaren är positionerad i ett skikt. Två numeriska exempel presenteras i slutet av rapporten.</p>		
<b>Nyckelord</b> elektromagnetisk, spridning, skiktad media, dyadiska greensfunktioner, dispersivt media		
<b>Övriga bibliografiska uppgifter</b>	<b>Språk</b> Engelska	
<b>ISSN</b> 1650-1942	<b>Antal sidor:</b> 24 s.	
<b>Distribution enligt missiv</b>	<b>Pris:</b> Enligt prislista	

## **Contents**

Problem formulation .....	1
The integral representations .....	3
The BEM discretisation.....	7
Scatterer crossing layer boundary interfaces.....	9
Division of faces.....	9
Outstretched triangles and their origin .....	11
Midpoints .....	12
Alternative solution to mesh refinement .....	12
The nodes on the boundary interface. ....	12
Numerical examples .....	13
Convergence of the BEM code .....	13
Future verification and evaluation.....	15
Buried large scatterer .....	15
Scattering caused by the electric background field.....	18
Conclusions .....	23
Acknowledgement.....	23
References .....	24

## **Introduction**

Surface integral formulations have been used as a basis for programs to calculate electromagnetic scattering from smooth objects in dispersive media. FOI (The Swedish Defence Agency) has developed two different programs NLAYSCA [1] and EMS-BEM [2] using this method for extremely low frequencies (ELF). Neither of these two programs allows the scattering object to be positioned in more than one layer, and the object is assumed to be perfectly conducting. This paper describes the theory behind a new program named EMSCATT that allows the object to be placed anywhere in a stratified environment, which means the scattering object can be placed across layer interfaces.

The method used to solve the unknown current density on the surface is a Boundary Element Method (BEM) combined with point collocation. This method divides the surface of the scattering object into triangular elements where the unknown quantity is interpolated by an expansion in quadratic basis functions. The electric and magnetic fields outside the scattering object consists of the direct contribution from the source and the scattered fields from the reflecting object. The reflected fields are the contribution from the surface integral representations on the scattering object and consist of products between unknown tangential magnetic fields and the electric and magnetic dyadic Green's functions. The dyadic Green's functions are fundamental wave propagation solutions to a certain horizontally layered environment which makes the forms of the representations independent of the geometry. The fields from the source and the Green's functions are computed using code from the program NLAYER 2.0 [3]. A system of linear equations for the expansion coefficients are set up using point matching at each node. The system is solved using an algorithm for solving non symmetrical linear systems [4].

The convergence of the scattered fields from the program is evaluated and compared with the results from NLAYSCA. An approximation of the Dyadic Green's functions is examined and found to compute the collocation matrix in less than a sixth of the time it takes without the approximation.

Two different numerical examples of objects positioned in more than one layer are shown illustrating the use of the program and its limitations. The first example is a large scatterer in a three layer environment where the scatterer is positioned in the water and sediment layer. This example illustrates why mesh refinement is important when the source is close to the scatterer. The second numerical example is an evaluation of the shielding effects surface vessels have on the electric background field. The ship is approximated to be a perfectly conducting ellipsoid. The vessel will scatter the background producing an interference pattern around the ship with a measurable decrease of the field intensity directly below the ship.

## **Problem formulation**

Consider a smooth object in a horizontally layered environment, where the layers represent air, water, sediment, and bedrock. The object may be situated in more than one layer at a time and it is assumed that all media, layers and the scatterer, are nonmagnetic. Sources with the

time dependence  $e^{-i\omega t}$  can be placed anywhere in the environment, with the exception of the space occupied by the scatterer. The angular frequency is denoted by  $\omega$  and the time by  $t$ .

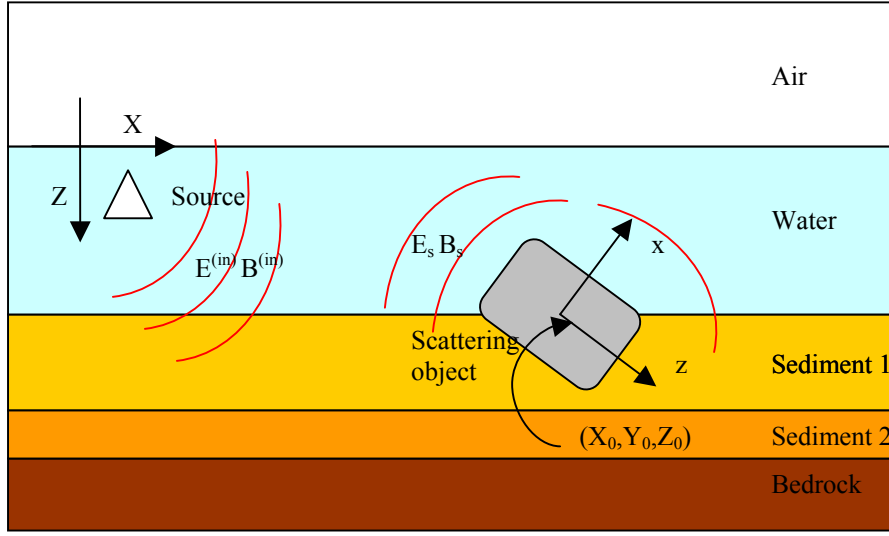


Figure 1. Example of a five layer environment.

The scattering object has a local coordinate system  $xyz$  which is attached at the point  $(X_0, Y_0, Z_0)$  in the environment  $XYZ$ . The relation between the right-handed coordinate systems is described by Euler angles as

$$\begin{bmatrix} x \\ y \\ z \end{bmatrix} = \mathbf{R} \begin{bmatrix} X - X_0 \\ Y - Y_0 \\ Z - Z_0 \end{bmatrix}, \quad \begin{bmatrix} X \\ Y \\ Z \end{bmatrix} = \mathbf{R}^T \begin{bmatrix} x \\ y \\ z \end{bmatrix} + \begin{bmatrix} X_0 \\ Y_0 \\ Z_0 \end{bmatrix} \quad (1)$$

where  $\mathbf{R}$  is the rotation matrix and is given in Euler angles as

$$\mathbf{R} = \begin{bmatrix} \cos \zeta & \sin \zeta & 0 \\ -\sin \zeta & \cos \zeta & 0 \\ 0 & 0 & 1 \end{bmatrix} \begin{bmatrix} \cos \eta & 0 & -\sin \eta \\ 0 & 1 & 0 \\ \sin \eta & 0 & \cos \eta \end{bmatrix} \begin{bmatrix} \cos \xi & \sin \xi & 0 \\ -\sin \xi & \cos \xi & 0 \\ 0 & 0 & 1 \end{bmatrix} \quad (2)$$

The superscript T denotes the transpose of R.

The vector wave equations for the electric and magnetic fields are

$$\left. \begin{aligned} \nabla \times \nabla \times \mathbf{E}_j(\mathbf{r}) - k_j^2 \mathbf{E}_j(\mathbf{r}) &= i\omega \mu_0 \mathbf{J}_j(\mathbf{r}) \delta_{ij} \\ \nabla \times \nabla \times \mathbf{H}_j(\mathbf{r}) - k_j^2 \mathbf{H}_j(\mathbf{r}) &= \nabla \times \mathbf{J}_j(\mathbf{r}) \delta_{ij} \end{aligned} \right\}, \quad i \text{ index of the layer the source is in} \quad (3)$$

with the wave numbers

$$k_j = \omega \sqrt{\mu_0 \epsilon_0 \left( 1 + \frac{i\sigma_j}{\omega \epsilon_j} \right)}, \quad \text{Re}(k_j \geq 0). \quad (4)$$

The permeability in vacuum is denoted by  $\mu_0$  and the permittivity and conductivity in the regions are  $\varepsilon_j$  and  $\sigma_j$  respectively,  $j$  is the index of the layer the field point is in. The free volume current density is denoted  $\mathbf{J}(\mathbf{r})$ .

The boundary conditions on a perfectly conducting scatterer are

$$\mathbf{n} \times (\mathbf{E}) = 0, \quad \mathbf{n} \times (\mathbf{H}) = \mathbf{K}, \quad \mathbf{n} \cdot (\varepsilon \mathbf{E}) = \rho_s, \quad \mathbf{n} \cdot (\mathbf{H}) = 0 \quad (5)$$

where  $\mathbf{n}$  is the inward pointing unit normal to the object surface. The vector  $\mathbf{K}$  is the surface current density and the scalar  $\rho_s$  is the charge density.

The boundary conditions at the interfaces between the regions are

$$\left. \begin{aligned} \hat{\mathbf{e}}_z \times (\mathbf{E}^+ - \mathbf{E}^-) = 0, \quad \hat{\mathbf{e}}_z \times (\mathbf{H}^+ - \mathbf{H}^-) = 0 \\ \hat{\mathbf{e}}_z \cdot (\varepsilon_+ \mathbf{E}^+ - \varepsilon_- \mathbf{E}^-) = 0, \quad \hat{\mathbf{e}}_z \cdot (\mathbf{H}^+ - \mathbf{H}^-) = 0 \end{aligned} \right\} \quad (6)$$

The radiation conditions for the  $\mathbf{E}$ - and  $\mathbf{H}$ - fields are satisfied at infinity and are

$$\lim_{r \rightarrow \infty} r [\nabla \times \mathbf{E}(\mathbf{r}) - ik_j \hat{\mathbf{e}}_r \times \mathbf{E}(\mathbf{r})] = 0, \quad \lim_{r \rightarrow \infty} r [\nabla \times \mathbf{H}(\mathbf{r}) - ik_j \hat{\mathbf{e}}_r \times \mathbf{H}(\mathbf{r})] = 0 \quad (7)$$

## The integral representations

To formulate an integral equation that can solve general problems without treatment of special cases it is convenient to use dyadic Green's functions. The electric dyadic Green's function  $\overline{\overline{G}}_e$  and the magnetic dyadic Green's function  $\overline{\overline{G}}_m$  are problem dependent. They are fundamental solutions to dipole sources in the medium when the scatterer isn't present. The dyadic  $\overline{\overline{G}}_e$  contains the three electric field solutions to three sources which are normalized infinitesimal current dipoles in three mutual perpendicular directions located at  $\mathbf{r}'$ . The dyadic  $\overline{\overline{G}}_m$  contains the magnetic fields to these sources. See [5] for more information about dyadic Green's functions. The wave equations for  $\overline{\overline{G}}_e$  and  $\overline{\overline{G}}_m$  are

$$\left. \begin{aligned} \nabla \times \nabla \times \overline{\overline{G}}_{ej}(\mathbf{r}, \mathbf{r}') - k_j^2 \overline{\overline{G}}_{ej}(\mathbf{r}, \mathbf{r}') &= \overline{\overline{I}} \delta(\mathbf{r} - \mathbf{r}') \delta_{ij} \\ \nabla \times \nabla \times \overline{\overline{G}}_{mj}(\mathbf{r}, \mathbf{r}') - k_j^2 \overline{\overline{G}}_{mj}(\mathbf{r}, \mathbf{r}') &= \nabla \times \left[ \overline{\overline{I}} \delta(\mathbf{r} - \mathbf{r}') \right] \delta_{ij} \end{aligned} \right\}, \quad i, \text{ index of the layer the source is in} \quad (8)$$

where  $\overline{\overline{I}}$  is the unit diagonal dyadic and  $\delta(\mathbf{r} - \mathbf{r}')$  the Dirac delta function. The boundary conditions at the regions interfaces for  $\overline{\overline{G}}_e$  and  $\overline{\overline{G}}_m$  are the same as for the  $\mathbf{E}$ - and  $\mathbf{H}$ -fields.

$$\left. \begin{aligned} \hat{e}_z \times \left( \overline{\overline{G}}_e(\mathbf{r}^+, \mathbf{r}') - \overline{\overline{G}}_e(\mathbf{r}^-, \mathbf{r}') \right) = 0 \quad , \quad \hat{e}_z \times \left( \overline{\overline{G}}_m(\mathbf{r}^+, \mathbf{r}') - \overline{\overline{G}}_m(\mathbf{r}^-, \mathbf{r}') \right) = 0 \\ \hat{e}_z \cdot \left( \varepsilon_+ \overline{\overline{G}}_e(\mathbf{r}^+, \mathbf{r}') - \varepsilon_- \overline{\overline{G}}_e(\mathbf{r}^-, \mathbf{r}') \right) = 0 \quad , \quad \hat{e}_z \cdot \left( \overline{\overline{G}}_m(\mathbf{r}^+, \mathbf{r}') - \overline{\overline{G}}_m(\mathbf{r}^-, \mathbf{r}') \right) = 0 \end{aligned} \right\} \quad (9)$$

The integral representations for the  $\mathbf{E}$ - field are derived from equation (3) and (8) in the following way  $\mathbf{E}(\mathbf{r}) \cdot (8) - (3) \cdot \overline{\overline{G}}_e(\mathbf{r}) \Rightarrow$

$$\begin{aligned} \mathbf{E}(\mathbf{r})\delta(\mathbf{r} - \mathbf{r}') - i\omega\mu_0\mathbf{J}(\mathbf{r})\overline{\overline{G}}_e(\mathbf{r}, \mathbf{r}') = \\ \mathbf{E}(\mathbf{r}) \cdot (\nabla \times \nabla \times \overline{\overline{G}}_e(\mathbf{r}, \mathbf{r}')) - (\nabla \times \nabla \times \mathbf{E}(\mathbf{r})) \cdot \overline{\overline{G}}_e(\mathbf{r}, \mathbf{r}') \end{aligned} \quad (10)$$

Integrate (10) over the space  $V$  surrounding the scatterer and the source. The boundary conditions for the Green's functions allow the volume  $V$  to incorporate multiple layers.

$$\begin{aligned} \int_V \mathbf{E}(\mathbf{r})\delta(\mathbf{r} - \mathbf{r}') - i\omega\mu_0\mathbf{J}(\mathbf{r})\overline{\overline{G}}_e(\mathbf{r}, \mathbf{r}')dV(\mathbf{r}) = \\ \int_V \mathbf{E}(\mathbf{r}) \cdot (\nabla \times \nabla \times \overline{\overline{G}}_e(\mathbf{r}, \mathbf{r}')) - (\nabla \times \nabla \times \mathbf{E}(\mathbf{r})) \cdot \overline{\overline{G}}_e(\mathbf{r}, \mathbf{r}')dV(\mathbf{r}) \end{aligned} \quad (11)$$

The term containing the free current density in the left hand side of equation (11) represents the incoming field  $\mathbf{E}^{(in)}(\mathbf{r}')$  and after using  $\nabla \times \mathbf{E}(\mathbf{r}) = i\omega\mu_0\mathbf{H}(\mathbf{r})$  ,  $\nabla \times \overline{\overline{G}}_e(\mathbf{r}, \mathbf{r}') = \overline{\overline{G}}_m(\mathbf{r}, \mathbf{r}')$  and the second vector-dyadic Green's theorem

$$\iiint_V \left[ \mathbf{P} \cdot (\nabla \times \nabla \times \overline{\overline{Q}}) - (\nabla \times \nabla \times \mathbf{P}) \cdot \overline{\overline{Q}} \right] dV = - \iint_S \left[ (\mathbf{n} \times \nabla \times \mathbf{P}) \cdot \overline{\overline{Q}} + (\mathbf{n} \times \mathbf{P}) \cdot (\nabla \times \overline{\overline{Q}}) \right] dS \quad (12)$$

where  $\mathbf{n}$  is the outward unit normal to the surface  $S$  enclosing the volume  $V$  equation (11) becomes

$$\mathbf{E}(\mathbf{r}') = \mathbf{E}^{(in)}(\mathbf{r}') - \int_{S_{scatt}} i\omega\mu_0(\mathbf{n}(\mathbf{r}) \times \mathbf{H}(\mathbf{r})) \cdot \overline{\overline{G}}_e(\mathbf{r}, \mathbf{r}') + (\mathbf{n}(\mathbf{r}) \times \mathbf{E}(\mathbf{r})) \cdot \overline{\overline{G}}_m(\mathbf{r}, \mathbf{r}')dS(\mathbf{r}), \quad \mathbf{r}' \notin V_{scatt} \quad (13)$$

The volume  $V$  is bounded by two surfaces, an inner surface  $S_{scatt}$  enclosing the scatterer and an outer surface  $S_{inf}$  surrounding the whole volume  $V$  at infinity. The contributions from the surface integral  $S_{inf}$  vanishes due to the radiation condition (7). Equation (13) uses  $\mathbf{r}'$  to represent the field point,  $\mathbf{r}$  is commonly used for the source point, therefore  $\mathbf{r}$  is interchanged with  $\mathbf{r}'$  and the expression becomes

$$\mathbf{E}(\mathbf{r}) = \mathbf{E}^{(in)}(\mathbf{r}) - \int_{S_{scatt}} i\omega\mu_0(\mathbf{n}(\mathbf{r}') \times \mathbf{H}(\mathbf{r}')) \cdot \overline{\overline{G}}_e(\mathbf{r}', \mathbf{r}) + (\mathbf{n}(\mathbf{r}') \times \mathbf{E}(\mathbf{r}')) \cdot \overline{\overline{G}}_m(\mathbf{r}', \mathbf{r})dS(\mathbf{r}'), \quad \mathbf{r} \notin V_{scatt} \quad (14)$$

which follows the common notation for field expressions. The expression for the  $\mathbf{H}$ -field can be derived in a similar way yielding

$$\mathbf{H}(\mathbf{r}) = \mathbf{H}^{(\text{in})}(\mathbf{r}) - \int_{S_{\text{scatt}}} (\mathbf{n}(\mathbf{r}') \times \mathbf{H}(\mathbf{r}')) \cdot \overline{\overline{\mathbf{G}}}_m(\mathbf{r}', \mathbf{r}) + i\omega\epsilon(\mathbf{n}(\mathbf{r}') \times \mathbf{E}(\mathbf{r}')) \cdot \overline{\overline{\mathbf{G}}}_e(\mathbf{r}', \mathbf{r}) dS(\mathbf{r}'), \quad \mathbf{r} \notin V_{\text{scatt}} \quad (15)$$

To derive the fields inside the scatterer the dyadic Green's functions  $\overline{\overline{\mathbf{G}}}_{e0}(\mathbf{r}', \mathbf{r})$  and  $\overline{\overline{\mathbf{G}}}_{m0}(\mathbf{r}', \mathbf{r})$  are used which are the whole space dyadic Green's functions. With the exception that the volume  $V$  is the volume  $V_{\text{scatt}}$  occupied by the scatterer and that  $\mathbf{n}$  is the inward unit normal.

$$\mathbf{E}(\mathbf{r}) = \int_{S_{\text{scatt}}} i\omega\mu_0(\mathbf{n}(\mathbf{r}') \times \mathbf{H}(\mathbf{r}')) \cdot \overline{\overline{\mathbf{G}}}_{e0}(\mathbf{r}', \mathbf{r}) + (\mathbf{n}(\mathbf{r}') \times \mathbf{E}(\mathbf{r}')) \cdot \overline{\overline{\mathbf{G}}}_{m0}(\mathbf{r}', \mathbf{r}) dS(\mathbf{r}') \quad , \quad \mathbf{r} \in V_{\text{scatt}} \quad (16)$$

$$\mathbf{H}(\mathbf{r}) = \int_{S_{\text{scatt}}} (\mathbf{n}(\mathbf{r}') \times \mathbf{H}(\mathbf{r}')) \cdot \overline{\overline{\mathbf{G}}}_{m0}(\mathbf{r}', \mathbf{r}) + i\omega\epsilon(\mathbf{n}(\mathbf{r}') \times \mathbf{E}(\mathbf{r}')) \cdot \overline{\overline{\mathbf{G}}}_{e0}(\mathbf{r}', \mathbf{r}) dS(\mathbf{r}') \quad , \quad \mathbf{r} \in V_{\text{scatt}} \quad (17)$$

For a perfectly conducting scatterer the fields inside the object are zero. Hence, using the boundary conditions (5) the integral representations (14) – (17) become

$$\begin{aligned} \mathbf{E}(\mathbf{r}) &= \mathbf{E}^{(\text{in})}(\mathbf{r}) - \int_{S_{\text{scatt}}} i\omega\mu_0 \mathbf{K}(\mathbf{r}') \cdot \overline{\overline{\mathbf{G}}}_e(\mathbf{r}', \mathbf{r}) dS(\mathbf{r}') \\ \mathbf{H}(\mathbf{r}) &= \mathbf{H}^{(\text{in})}(\mathbf{r}) - \int_{S_{\text{scatt}}} \mathbf{K}(\mathbf{r}') \cdot \overline{\overline{\mathbf{G}}}_m(\mathbf{r}', \mathbf{r}) dS(\mathbf{r}') \end{aligned} \quad , \quad \mathbf{r} \notin V_{\text{scatt}} \quad (18)$$

$$\begin{aligned} \mathbf{E}(\mathbf{r}) &= 0 \\ \mathbf{H}(\mathbf{r}) &= 0 \end{aligned} \quad , \quad \mathbf{r} \in V_{\text{scatt}} \quad (19)$$

To solve for the unknown surface current density  $\mathbf{K}$  on the scatterer an integral equation of the second kind is derived. The integral equation of the second kind is obtained by operating with  $\mathbf{n}(\mathbf{r}) \times$  from the left on the  $\mathbf{H}$ - field representation in (18) and letting  $\mathbf{r} \rightarrow S_{\text{scatt}}$  from the outside of the surface. This limit yields

$$\frac{1}{2} \mathbf{K}(\mathbf{r}) + \int_{S_{\text{scatt}}} \mathbf{n}(\mathbf{r}) \times (\mathbf{K}(\mathbf{r}') \cdot \overline{\overline{\mathbf{G}}}_m(\mathbf{r}', \mathbf{r})) dS(\mathbf{r}') = \mathbf{K}^{(\text{in})}(\mathbf{r}) \quad , \quad \mathbf{r} \in S_{\text{scatt}} \quad (20)$$

which is an integral equation of the second kind for  $\mathbf{K}$ . The surface  $S_{\text{scatt}}$  is assumed to be smooth. The analogous limiting procedure on the  $\mathbf{H}$ - field representation for a whole-space is performed in [8].

To be able to solve (20) a scalar version of the equation is formed. The surface current density vector is tangential on the surface  $S_{\text{scatt}}$  and can therefore be composed as  $\mathbf{K}(\mathbf{r}) = \hat{e}_s K_s(\mathbf{r}) + \hat{e}_t K_t(\mathbf{r})$  where  $\hat{e}_s$  and  $\hat{e}_t$  are to unit tangential vectors at a point  $\mathbf{r}$  on  $S_{\text{scatt}}$ . The integral equation (20) is then projected onto these vectors at the point  $\mathbf{r}$ . The result is

$$\begin{aligned} \frac{1}{2} K_s(\mathbf{r}) + \int_{S_{\text{scatt}}} Q_{m11}(\mathbf{r}', \mathbf{r}) K_s(\mathbf{r}') + Q_{m12}(\mathbf{r}', \mathbf{r}) K_t(\mathbf{r}') dS &= K_s^{(\text{in})}(\mathbf{r}) \\ \frac{1}{2} K_t(\mathbf{r}) + \int_{S_{\text{scatt}}} Q_{m21}(\mathbf{r}', \mathbf{r}) K_s(\mathbf{r}') + Q_{m22}(\mathbf{r}', \mathbf{r}) K_t(\mathbf{r}') dS &= K_t^{(\text{in})}(\mathbf{r}) \end{aligned} \quad (21)$$

where

$$\begin{aligned} Q_{1i}(\mathbf{r}, \mathbf{r}') &= \sum_{j=1}^3 e_{sj}(\mathbf{r}') B_{ij}(\mathbf{r}, \mathbf{r}') \\ Q_{2i}(\mathbf{r}, \mathbf{r}') &= \sum_{j=1}^3 e_{tj}(\mathbf{r}') B_{ij}(\mathbf{r}, \mathbf{r}') \end{aligned} \quad (22)$$

The vector components  $e_{sj}$  and  $e_{tj}$  are defined as

$$\begin{aligned} \mathbf{e}_s(\mathbf{r}) &= \hat{e}_x e_{s1}(\mathbf{r}) + \hat{e}_y e_{s2}(\mathbf{r}) + \hat{e}_z e_{s3}(\mathbf{r}) \\ \mathbf{e}_t(\mathbf{r}) &= \hat{e}_x e_{t1}(\mathbf{r}) + \hat{e}_y e_{t2}(\mathbf{r}) + \hat{e}_z e_{t3}(\mathbf{r}) \end{aligned} \quad (23)$$

and the functions  $B_{ij}(\mathbf{r}, \mathbf{r}')$  are derived

$$\begin{aligned} B_{i1}(\mathbf{r}, \mathbf{r}') &= n_2(\mathbf{r}') C_{i3}(\mathbf{r}, \mathbf{r}') - n_3(\mathbf{r}') C_{i2}(\mathbf{r}, \mathbf{r}') \\ B_{i2}(\mathbf{r}, \mathbf{r}') &= n_3(\mathbf{r}') C_{i1}(\mathbf{r}, \mathbf{r}') - n_1(\mathbf{r}') C_{i3}(\mathbf{r}, \mathbf{r}') \\ B_{i3}(\mathbf{r}, \mathbf{r}') &= n_1(\mathbf{r}') C_{i2}(\mathbf{r}, \mathbf{r}') - n_2(\mathbf{r}') C_{i1}(\mathbf{r}, \mathbf{r}') \end{aligned} \quad (24)$$

where

$$\begin{aligned} C_{1k}(\mathbf{r}, \mathbf{r}') &= \sum_{j=1}^3 e_{sj}(\mathbf{r}) G_{kj}(\mathbf{r}, \mathbf{r}') \\ C_{2k}(\mathbf{r}, \mathbf{r}') &= \sum_{j=1}^3 e_{tj}(\mathbf{r}) G_{kj}(\mathbf{r}, \mathbf{r}') \end{aligned} \quad (25)$$

The normal vector components  $n_j$  are defined by

$$\mathbf{n}(\mathbf{r}) = e_x n_1(\mathbf{r}) + e_y n_2(\mathbf{r}) + e_z n_3(\mathbf{r}) \quad (26)$$

The electric and the magnetic Green's dyadic elements  $G_{eij}(\mathbf{r}, \mathbf{r}')$  and  $G_{mij}(\mathbf{r}, \mathbf{r}')$  are defined as

$$\begin{aligned} \overline{\overline{G}}_e(\mathbf{r}, \mathbf{r}') &= \sum_{i=1}^3 \sum_{j=1}^3 G_{eij}(\mathbf{r}, \mathbf{r}') e_i e_j \\ \overline{\overline{G}}_m(\mathbf{r}, \mathbf{r}') &= \sum_{i=1}^3 \sum_{j=1}^3 G_{mij}(\mathbf{r}, \mathbf{r}') e_i e_j \\ e_1 &= \hat{e}_x, e_2 = \hat{e}_y, e_3 = \hat{e}_z \end{aligned} \quad (27)$$

The equations for the field expressions (18) outside the scatterer can be projected onto  $e_i$  resulting in six scalar equations.

$$\begin{aligned}
 E_i(\mathbf{r}) &= E_i^{\text{in}}(\mathbf{r}) - i\omega\mu_0 \int_{S_{\text{scatt}}} \sum_{j=1}^3 e_{sj}(\mathbf{r}) G_{ejj}(\mathbf{r}', \mathbf{r}) K_s(\mathbf{r}') dS(\mathbf{r}') - i\omega\mu_0 \int_{S_{\text{scatt}}} \sum_{j=1}^3 e_{tj}(\mathbf{r}) G_{tji}(\mathbf{r}', \mathbf{r}) K_t(\mathbf{r}') dS(\mathbf{r}') \\
 H_i(\mathbf{r}) &= H_i^{\text{in}}(\mathbf{r}) - \int_{S_{\text{scatt}}} \sum_{j=1}^3 e_{sj}(\mathbf{r}) G_{mji}(\mathbf{r}', \mathbf{r}) K_s(\mathbf{r}') dS(\mathbf{r}') - \int_{S_{\text{scatt}}} \sum_{j=1}^3 e_{tj}(\mathbf{r}) G_{mji}(\mathbf{r}', \mathbf{r}) K_t(\mathbf{r}') dS(\mathbf{r}')
 \end{aligned}$$

$\mathbf{r} \notin V_{\text{scatt}}, i = 1, 2, 3$

(28)

## The BEM discretisation

To solve the coupled scalar integral equations (21) a boundary element method is used, commonly referred to as BEM. The method, developed by K. E. Atkinson [6], divides the surface  $S$  into  $N$  triangles  $\Delta S_k$

$$S = \bigcup_{k=1}^N \Delta S_k \tag{29}$$

and the unknown functions are expanded in quadratic basis functions over the subsurface  $\Delta S_k$ . To create a linear system of equations collocation or point matching at the node points on the discretised surface is performed. Each element  $\Delta S_k$  has six node points, one in each corner and one connected to the midpoint of the side of each side of  $\Delta S_k$ . The six node points are parameterised by a one to one mapping function  $\mathbf{r} = \mathbf{m}_k(s, t)$ , figure 2.

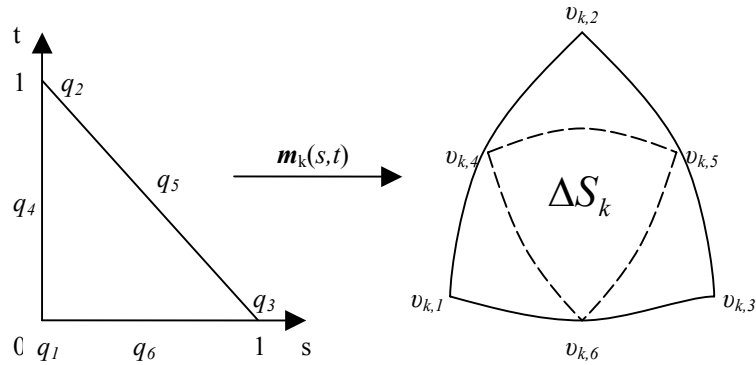


Figure 2. The parameterisation.

The six node points in a face  $\Delta S_k$  are denoted by  $v_{k,j}$  and they are mapped from the points  $q_j$  in the parameterisation domain  $\sigma$ . The nodes in the triangulation are denoted  $v_i$  and there are  $N_v = 2N + 2$  nodes in total. The triangulation is built by a mesh generator that produces a simple surface consisting out of four, eight or twenty faces. To produce a more detailed mesh each face  $\Delta S_k$  is divided in four new smaller elements as indicated by the dotted lines in figure 2. An other mesh generator is possible to implement as long as it produces triangular elements

that are joined at the edges and have midpoints specified. An example of a BEM mesh is displayed in figure 3.

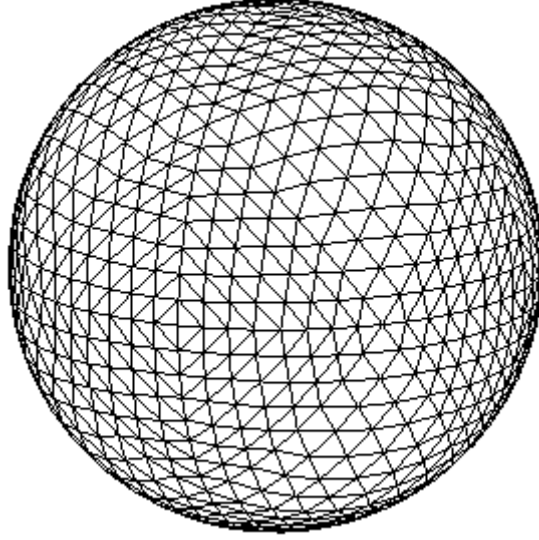


Figure 3. An example of a BEM mesh consisting of 512 faces.

The mapping function  $\mathbf{m}_k(s,t)$  is approximated by the expansion

$$\mathbf{m}_k(s,t) \approx \sum_{j=1}^6 \nu_{k,j} l_j(s,t), \quad (s,t) \in \sigma \quad (30)$$

where  $l_j(s,t)$  are the quadratic basis functions, for quadratic interpolation over  $\sigma$  at the interpolation points  $q_j$ . They are defined as

$$\begin{aligned} l_1(s,t) &= u(2u-1), \quad l_2(s,t) = t(2t-1), \quad l_3(s,t) = s(2s-1) \\ l_4(s,t) &= 4tu, \quad l_5(s,t) = 4st, \quad l_6(s,t) = 4su, \quad u = 1-s-t \end{aligned} \quad (31)$$

The surface current density components  $K_s$  and  $K_t$  using the expansion in (31) becomes

$$K_s(\mathbf{m}_k(s,t)) \approx \sum_{j=1}^6 K_s(\nu_{k,j}) l_j(s,t), \quad K_t(\mathbf{m}_k(s,t)) \approx \sum_{j=1}^6 K_t(\nu_{k,j}) l_j(s,t) \quad (32)$$

where the expansion coefficients are the surface current density vector at the node points. See [6] regarding details.

A linear system of equations for the unknowns is obtained by inserting the expansions (30) and (31) into the system of integral equations (21) and then performing collocation at the node points. This result in

$$\begin{aligned}
\frac{1}{2}K_s(\nu_i) + \sum_{k=1}^N \sum_{j=1}^6 Q_{11}^{kj}(\nu_i)K_s(\nu_{k,j}) + \sum_{k=1}^N \sum_{j=1}^6 Q_{12}^{kj}(\nu_i)K_t(\nu_{k,j}) &= K_s^{(in)}(\nu_i) \\
\frac{1}{2}K_t(\nu_i) + \sum_{k=1}^N \sum_{j=1}^6 Q_{21}^{kj}(\nu_i)K_s(\nu_{k,j}) + \sum_{k=1}^N \sum_{j=1}^6 Q_{22}^{kj}(\nu_i)K_t(\nu_{k,j}) &= K_t^{(in)}(\nu_i)
\end{aligned} \tag{33}$$

$i = 1, \dots, N_\nu$

where the collocation integrals  $Q_{mm'}^{kj}$  are

$$Q_{mm'}^{kj}(\nu_i) = \int_{\sigma} Q_{mm'}(\mathbf{m}_k(s,t), \nu_i) l_j(s,t) |D_s \mathbf{m}_k \times D_t \mathbf{m}_k| d\sigma \tag{34}$$

$$D_s \mathbf{m}_k = \frac{\partial \mathbf{m}_k(s,t)}{\partial s}, \quad D_t \mathbf{m}_k = \frac{\partial \mathbf{m}_k(s,t)}{\partial t} \tag{35}$$

The BEM discretisation in the integral representation (28) yields

$$\begin{aligned}
E_i(\mathbf{r}) &= E_i^{(in)}(\mathbf{r}) - i\omega\mu_0 \sum_{k=1}^N \sum_{j=1}^6 K_s(\nu_{k,j}) G_{ee's}^{kj}(\mathbf{r}) - i\omega\mu_0 \sum_{k=1}^N \sum_{j=1}^6 K_t(\nu_{k,j}) G_{ee't}^{kj}(\mathbf{r}) \\
H_i(\mathbf{r}) &= H_i^{(in)}(\mathbf{r}) - \sum_{k=1}^N \sum_{j=1}^6 K_s(\nu_{k,j}) G_{mm's}^{kj}(\mathbf{r}) - \sum_{k=1}^N \sum_{j=1}^6 K_t(\nu_{k,j}) G_{mm't}^{kj}(\mathbf{r})
\end{aligned} \tag{36}$$

$$\mathbf{r} \notin V, \quad i = 1, 2, 3$$

where  $G_{ee's}^{kj}$ ,  $G_{ee't}^{kj}$ ,  $G_{mm's}^{kj}$  and  $G_{mm't}^{kj}$  are

$$\begin{aligned}
G_{ee's}^{kj}(\mathbf{r}) &= \int_{\sigma} \sum_{l=1}^3 e_{sl}(\mathbf{m}_k(s,t)) G_{eli}(\mathbf{m}_k(s,t), \mathbf{r}) l_j(s,t) |D_s \mathbf{m}_k \times D_t \mathbf{m}_k| d\sigma \\
G_{ee't}^{kj}(\mathbf{r}) &= \int_{\sigma} \sum_{l=1}^3 e_{tl}(\mathbf{m}_k(s,t)) G_{eli}(\mathbf{m}_k(s,t), \mathbf{r}) l_j(s,t) |D_s \mathbf{m}_k \times D_t \mathbf{m}_k| d\sigma \\
G_{mm's}^{kj}(\mathbf{r}) &= \int_{\sigma} \sum_{l=1}^3 e_{sl}(\mathbf{m}_k(s,t)) G_{mli}(\mathbf{m}_k(s,t), \mathbf{r}) l_j(s,t) |D_s \mathbf{m}_k \times D_t \mathbf{m}_k| d\sigma \\
G_{mm't}^{kj}(\mathbf{r}) &= \int_{\sigma} \sum_{l=1}^3 e_{tl}(\mathbf{m}_k(s,t)) G_{mli}(\mathbf{m}_k(s,t), \mathbf{r}) l_j(s,t) |D_s \mathbf{m}_k \times D_t \mathbf{m}_k| d\sigma
\end{aligned} \tag{37}$$

## Scatterer crossing layer boundary interfaces

### Division of faces

The goal is to be able to compute the scattered fields from a scatterer that is positioned in more than one layer in the environment. If the scattering object is placed in more than one layer, this will have to be considered when the BEM approximations are made.

Analytically the integral in (20) is defined although the object cuts a layer boundary. The problem is numerical and occurs when the collocation integrals are computed for a face with node points that are positioned in different layers. The field on a face changes quickly over a boundary if the contrast between the mediums is high. Hence, it will result in that the collocation at the node points will produce an incorrect answer. The solution to this problem is to refine the mesh in such a way that the faces that have nodes in more than one layer are divided into smaller faces that only belong to one layer.

A face that needs to be divided will be split into three or two new faces depending on how it is positioned. If the corner nodes in a face lies in different layers and none of the corner nodes are positioned on a layer boundary the face will be divided by the layer boundary into a triangle and a quadrilateral. The quadrilateral is then cut along its shortest diagonal creating two triangles, see figure 4, creating three new triangles in total. If one corner in a face lies on the boundary and the other two nodes are positioned on different sides of the layer boundary the boundary layer will divide the face into two triangles, See figure 4.

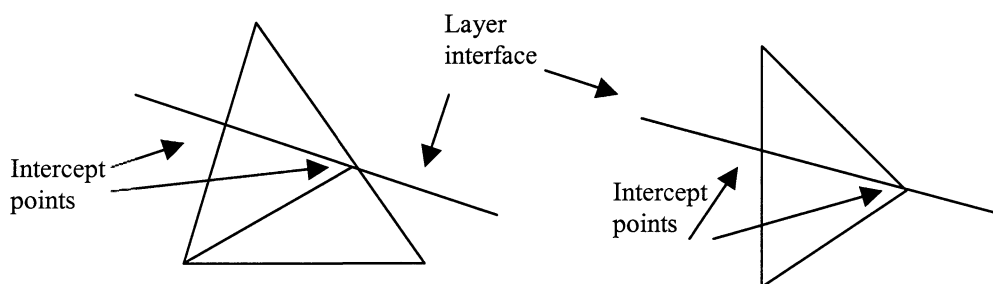


Figure 4. Division of faces.

To find intercept points where the sides of the faces meet the layer boundary an algorithm similar to the known search algorithm divide and conquer is used.

The algorithm first computes the midpoint between two corner nodes that are on opposite sides of a layer boundary. A new midpoint is then computed between the previously computed midpoint and the closest node on the other side of the boundary. If this is repeated the intercept point is found, see figure 5 for an illustration of the algorithm.

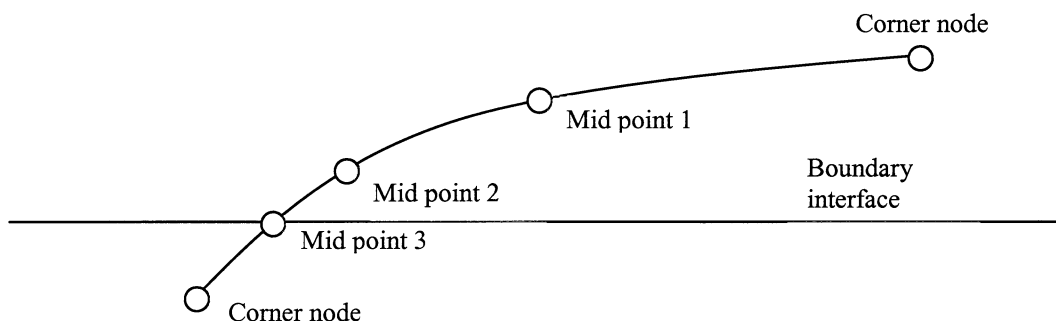


Figure 5. Illustration of algorithm to find the intercept point between two nodes.

This algorithm makes it possible to find the intercept point regardless of the scattering objects shape as long as there is a function that calculates the midpoint on the surface of the scattering

object between two nodes. Note that a midpoint between two nodes on i.e. a sphere isn't the same as for a plane.

### ***Outstretched triangles and their origin***

A problem that occurs when the triangular faces are divided is that it sometimes will create small or outstretched faces. The outstretched faces may give numerical errors and if they can be removed or prevented the number of faces that needs to be integrated over is reduced which will improve program performance. These faces are created when a small region of a face is divided by the algorithm described previously. The neighbouring faces of the resulting small triangle will share one side of the small triangle and most likely become long and outstretched, see figure 6.

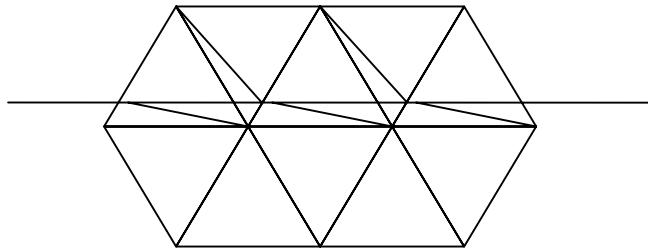


*Figure 6. Example of small and outstretched faces .*

To solve this problem small faces that have more than one node on the boundary interface are removed as well as their closest neighbours. A face is removed from the mesh when two nodes are in the same point. To remove a small face all nodes in the element are put in the same point on the boundary, this will result in that the faces next to the removed face will have two nodes in the same point and will be removed. See figure 7. After a face is removed new midpoints have to be computed for the faces in the mesh.

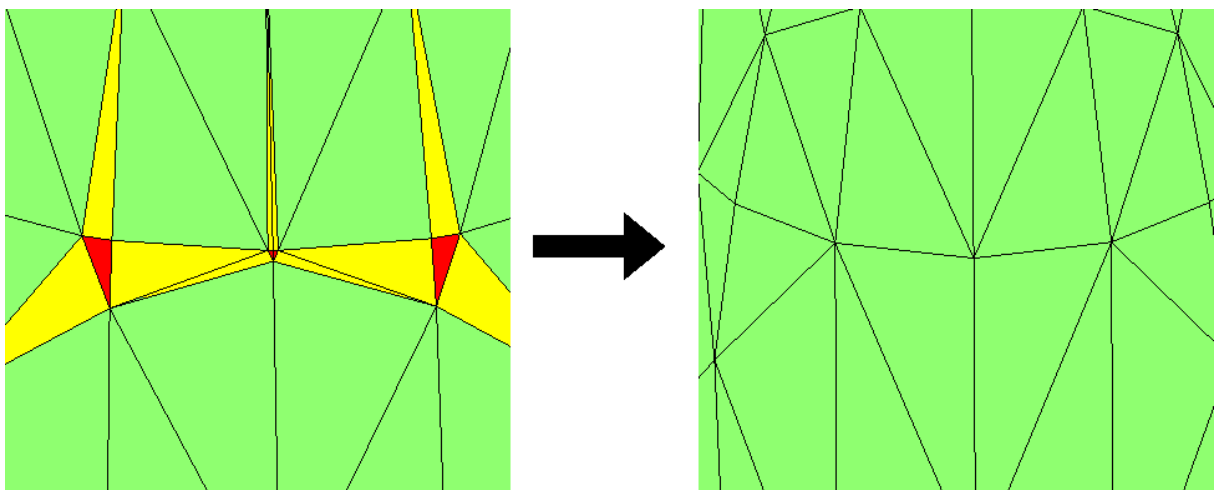


*Figure 7. Example of removal of small and outstretched faces, the small faces are coloured red and its neighbours are coloured yellow. (Midpoints are not shown in the figure)*

## ***Midpoints***

For each shape EMSCATT needs a specific function to compute the midpoints between two corner nodes. If a shape can't be described analytically the midpoint could be calculated using linear interpolation between the two nodes. Every shape also needs a function to compute the transversal and normal vectors to each node. To be able to use nonanalytical surfaces a method to compute the tangential and normal vectors at the nodes have to be used.

The function that computes the midpoints between two corners do not take any notice of layer boundaries. The result is that a midpoint may end up in the wrong layer. To prevent this problem, the midpoints are forced to be on the layer boundary, this is done finding intercept points or correcting the z-coordinate of the midpoint. If the resolution of the mesh is high these methods work well.

A problem that can occur is that the midpoint is placed in the wrong layer although both corner nodes, which the midpoint belongs to, are placed in the same layer. To solve this problem a new midpoint is calculated using linear interpolation, this is a rough approximation and often occurs when a face is outstretched and close to the layer interface. The easiest way to avoid these problems is to remove outstretched and small faces from the mesh.

## ***Alternative solution to mesh refinement***

In the previous discussion the faces that are positioned in more than two layers are divided into three or two new faces. If the mesh consists of many faces and a face only can be positioned in two layers moving the corner nodes to the layer boundary might be a better solution to the problem. This method would not create any small faces and probably less outstretched faces. This method could also be combined with the dividing method to move nodes that are close to a boundary and spitting the faces that are left.

## ***The nodes on the boundary interface.***

For a perfectly conducting scatterer only the surface current density needs to be calculated, and when doing so only the magnetic Green's dyad is used. These quantities are both dependent on the magnetic fields on the scatterer. The magnetic fields are continuous over the layer boundaries allowing nodes to be placed on the boundary or close to it. NLAYER which is the program used to compute the fields may have some problems computing the electric field when the contrast between two layers is high (i.e. air and water) for low frequencies and the result is that NLAYER gets stuck in a loop trying to achieve numerical convergence. To solve this it is wise to put the node in the layer which has the highest contrast, i.e. the nodes are put in the water layer if the layers are air and water. If the node can't be moved or NLAYER locks up anyway, the number of correct digits of the E and B field can be reduced to 4 or 5 digits (6 digits is the default value).

If the scatterer is a permeable scatterer the electric dyadic Green's functions and the tangential electric fields have to be considered on both sides for a node on the boundary to be able to

calculate the scattered fields. The electric fields are not continuous over the layer boundary and have to be calculated as a limit from either side. To do this the nodes on the boundary need to be split into two nodes with a distance  $\varepsilon$  from either side of the interface. The new nodes will create an equal amount of new equations and unknowns as there are new nodes. The result is that the size of the matrix containing the collocation integrals increases.

## Numerical examples

### Convergence of the BEM code

The program developed to solve scattering from a perfectly conducting object is named EMSCATT and is written in Fortran 95. The program is based on NLAYER 2.0 [3], a program which calculates the fields in a given point in the horizontally layered environment. NLAYER is used to compute the dyadic Green's functions and the incoming magnetic field  $\mathbf{H}^{(in)}$ . NLAYER can use different types of sources to produce the incoming fields. In the present configuration of NLAYER there are four main types of sources, electric dipoles, magnetic dipoles, electric line sources and magnetic loop sources, these sources can also be combined creating complex sources.

The BEM code in the program is based on a program EMS-BEM [2] and a program package from K. E. Atkinson [6]. The convergence of the BEM code is evaluated in [7] it has been found that for a whole space and a two layer environment 512 faces is more than sufficient to achieve a relative error smaller than 1%.

A convergence test for EMSCATT has been made in a four layer environment, where the layers represent air, water, sediment and bedrock. Layer data is specified in table 1.

	Layer thickness	Conductivity $\sigma$ [S/m]	Permittivity $\varepsilon_r$
Air	-	0	1
Water	20	0.800	81
Sediment	5	0.040	81
Bedrock	-	0.001	81

*Table 1. Layer data for convergence test*

The source is a horizontal electric dipole (HED) and is placed on a depth of 5m and points in the X-direction. A current moment of 50 Am and a frequency of 30 Hz is chosen. The scatterer is a sphere with a 5 m radius and is placed at a depth of 10 m and 50 m away from the source in the X-direction. The scattered fields are then computed along a straight path in the Y-direction at a depth of 10m and 30m away from the source in the X-direction. See figure 8.

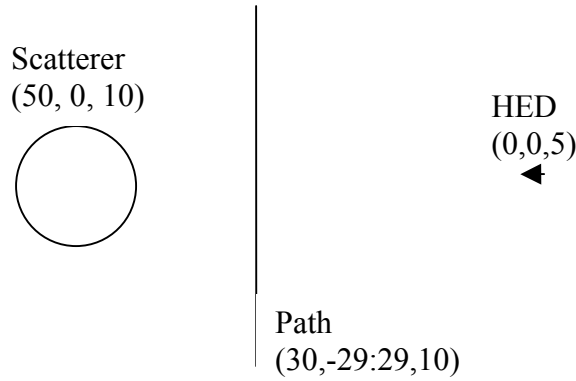


Figure 8. Source, scatterer and path positions.

The results are compared with calculated fields obtained from the program NLAYSCA [1]. NLAYSCA uses an earlier version of NLAYER for computations of the incoming fields and the dyadic Green's functions but instead of a BEM formulation this program uses Galerkin's method with spherical harmonic functions as basis functions. The relative error is plotted for the absolute values of the  $\mathbf{E}$ - and  $\mathbf{H}$ -fields in figure 9. The relative error is then calculated as

$$\frac{\left\| \mathbf{E}_{\text{EMSCATT}}^{\text{scatt}} - \mathbf{E}_{\text{NLAYSCA}}^{\text{scatt}} \right\|}{\left\| \mathbf{E}_{\text{NLAYSCA}}^{\text{scatt}} \right\|} \quad (38)$$

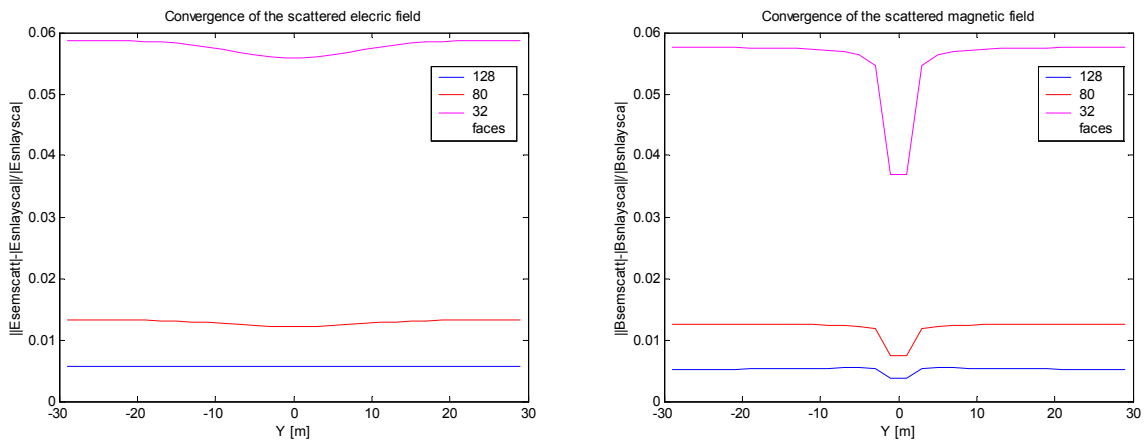


Figure 9. The convergence of the electromagnetic fields.

The relative error is below 1% for the scattered fields for 128 faces. This example took one hour to compute on a computer equipped with an Intel P4 processor running at 2.8 GHz. For a mesh consisting of 512 elements this time increases to approximately 16 hours. This is often too long and it would be desirable to make an approximation to make the calculation of the matrix containing the dyadic Green's functions faster.

A good approximation may be that the dyadic Green's function is constant in a face for a fine mesh. The approximation gives

$$Q_{mm'}^{kj}(\nu_i) = \int_{\sigma} Q_{mm'}(\mathbf{m}_k(\frac{1}{3}, \frac{1}{3}), \nu_i) \mathcal{I}_j(s, t) |D_s \mathbf{m}_k \times D_t \mathbf{m}_k| d\sigma \quad (39)$$

and will reduce the time to compute the collocation matrix to less than a sixth of the time it takes without the approximation. Now it is possible to calculate the collocation matrix for a mesh consisting of 320 faces in less time than it would take to calculate a mesh consisting of 128 faces without the use of the approximation. In figure 10 we can see that the relative fault is less for the mesh consisting of 320 faces and only slightly worse for the same mesh when the approximation is applied.

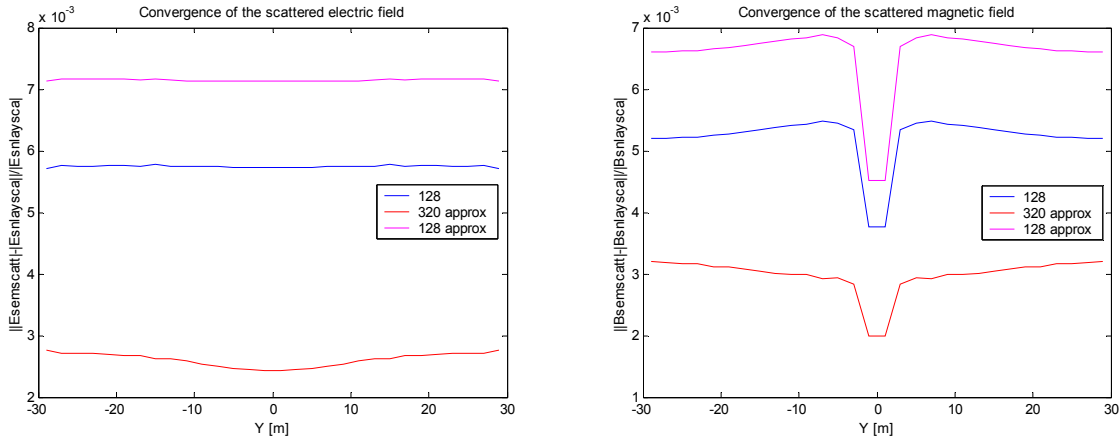


Figure 10. Approximation results compared to original code.

### Future verification and evaluation

Today there is no other program available to compute the scattered fields from a scatterer across a layer interface. In the future, programs or measured data will be used to verify and evaluate this program.

A detail that would be studied more is the computation of the dyadic Green's function. The function computing the dyadic Green's function uses a symmetrical relation that may not be completely accurate in a stratified environment for the magnetic dyadic Green's function. The impact of this error when computing the current density on the scatterer is not extensive because the matrix containing the collocation integral contributions is diagonally dominant. The scattered electric field will be very accurate since the equation only uses the electric dyadic function. The easiest way to detect an error in the dyadic Green's function would be to look at the scattered magnetic fields. A future evaluation and verification of this program should focus on the accuracy in the computation of the magnetic fields.

### Buried large scatterer

In this numerical example a large scatterer is positioned in the interface between the water and sediment layer in a three layer stratified environment described in table 2. The origin of the scattering object is positioned 25 m below the system origin. The scatterer is rotationally symmetric around the z-axis and the lower half of the scatterer is submerged in the sediment layer. The scatterer can be described as an ellipsoid with x-radii and y-radii set to 50 m and z-radii set to 10 m. The dimension of the scatterer will have some effects as seen in the results further on.

	Layer thickness	Conductivity $\sigma$ [S/m]	Permittivity $\epsilon_r$
Air	-	0	1
Water	25	0.800	81
Sediment	-	0.040	81

Table 2. Layer data for flat scatterer example

The source is a horizontal electric dipole with a moment of 50 Am and frequency of 3 Hz. It's directed in the x-direction and moved along a straight path from the coordinate (-800, 0, 3) to (210, 0, 3). The fields are computed for the point (200, 0, 24) one meter above the sediment layer. Field point, scattering position and source path is illustrated in figure 11.

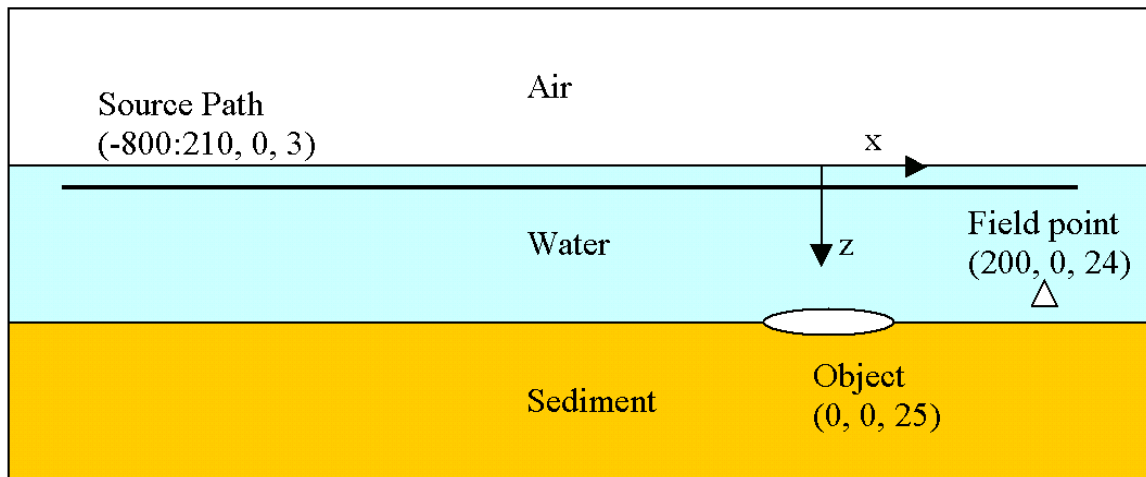


Figure 11. Source path, scatterer and field point positions in the three layer environment.

The scattered fields are computed for four different resolutions of the object mesh. The mesh refinement is very important when the source is close to the scatterer, since the node points then can be far apart compared to the source-scatterer distance. In figure 12a&b two meshes of the scattering object is shown, illustrating the node density of the surfaces. As seen in figure 13 the scattered fields converge for detailed meshes, but give unreliable results for the sparse mesh when the source is close to the scatterer.

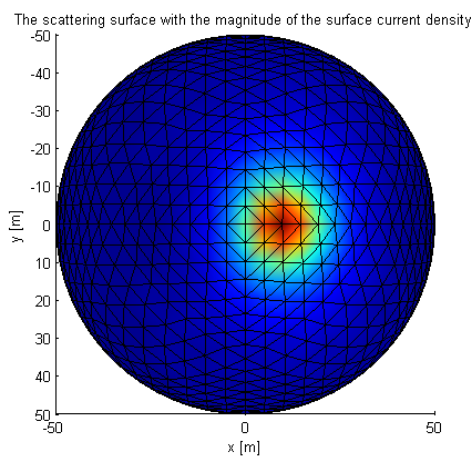


Figure 12a. Current density on scatterer of 512 faces. Source located at (10, 0, 3).

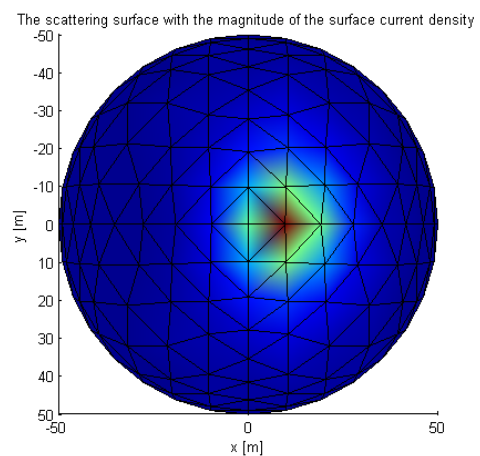


Figure 12b. Current density on scatterer of 128 faces. Source located at (10, 0, 3).

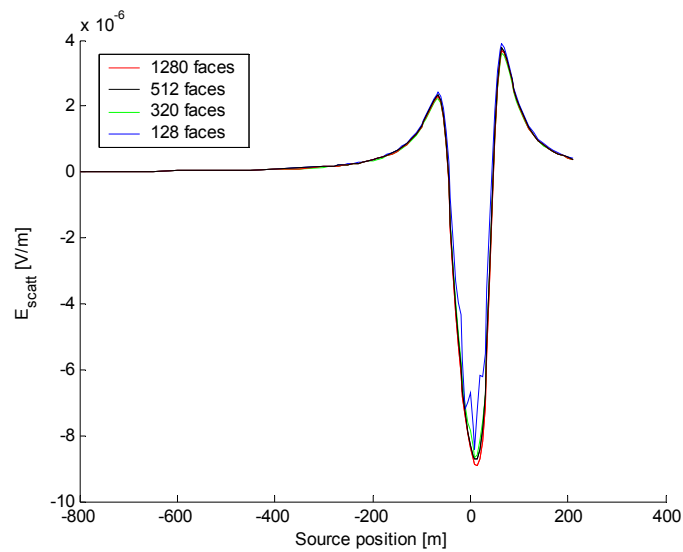


Figure 13. Scattered fields for four different meshes.

The field intensity in the field point is decreased when the source is above the scatterer compared to when the scatterer is absent in the environment as can be seen in figure 14. This is because the scatterer acts similar to a perfectly conducting plane when the source is directly above the scatterer. When there is a conducting plane present, the horizontal dipole can be replaced by an image of the dipole with the reverse direction which will cancel out the fields from the original source when the field point is far from the sources.

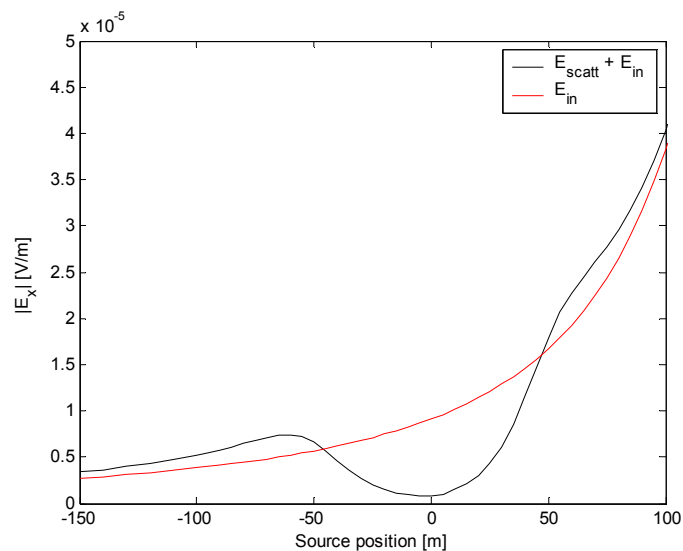


Figure 14. Dampening of the field when the scatterer is present.

When these examples were computed a four layer model was used instead of the three layer model stated earlier. The fourth layer was positioned below the sediment layer at a depth of 1000 m with the same material properties as the sediment layer. This was done because a bug in NLAYER 2.0 produced incorrect magnetic fields when the source is positioned in the third layer in a three layer environment. When the Dyadic Green's functions are computed in this example half of the source locations are positioned in the third layer and the result would be incorrect if a three layer environment was used.

## Scattering caused by the electric background field

In this numerical example scattering from surface vessels caused by the background is studied. The background is often considered as noise in most measurements but could also be used as a source in a scattering problem. A ship will create a scattered field close to the vessel that could be measured by a sensor at the bottom. The goal with this example is to illustrate this effect for three ship sized scattering objects.

The background consists of several different sources both natural and man made. At low frequencies the sources are mainly natural and at higher frequencies man made sources dominates. A spectrum of the background measured close to the bottom in the Swedish archipelago is presented in figure 15.

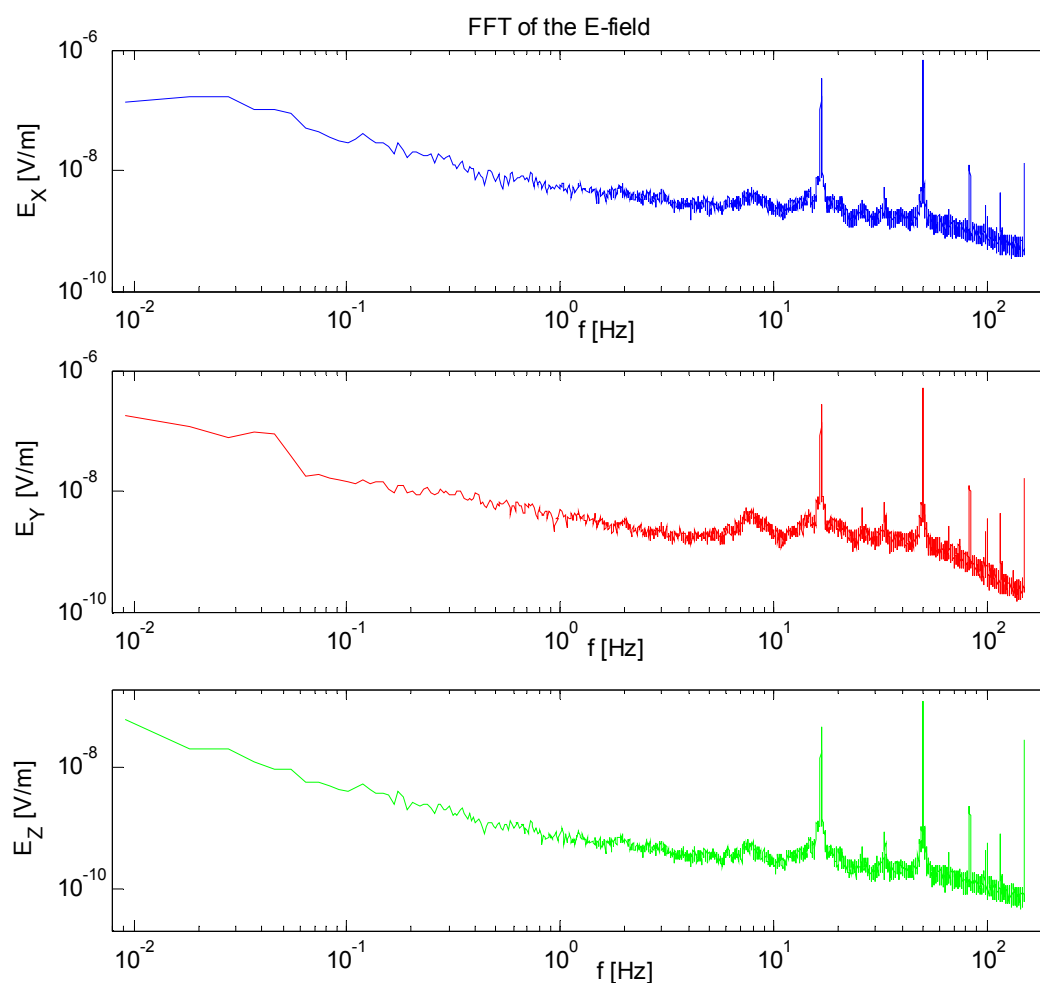


Figure 15. Frequency spectrum for fields measured close to bottom in the Swedish archipelago.

The background noise is strongest for frequencies lower than 1 Hz. At these frequencies the source of the background is a group of phenomena called micropulsations. Micropulsations create fields that originate from events in the ionosphere or the magnetosphere that are driven by the solar wind. The intensity of the micropulsations is approximately proportional to the

inverse of the signal frequency. If the goal is to measure changes in the background it might seem logical to measure signals at the lowest frequency possible. However, this is not the case. The system noise of measuring systems is often also proportional to the inverse of the frequency. Thus the signal to noise ratio does not change much for decreasing frequencies.

In figure 15. a peak at 8 Hz is clearly visible, this peak is the result of the first Schuman resonance. The Schuman resonances are the modes that are created in the resonance cavity in the atmosphere between the ionosphere and the surface of the earth. The resonance is fed by lightning strikes from thunderstorms. The first resonance frequency is near 8 Hz, the second around 14 Hz the third around 20 Hz [9]. These three resonances are visible in the spectrum in figure 15.

Around  $16^{2/3}$  Hz and 50 Hz there are two sharp peaks in the spectrum. These two frequencies are man made originating from power lines for the railroad and households respectively. In the archipelago these frequencies can be measured almost anywhere. This is because the power lines are grounded on islands creating currents between the islands and the mainland. The harmonics of these frequencies can also be strong i.e. contributions from 150 Hz is present in the frequency spectrum in figure 15.

To simulate something that could be similar to the background a horizontal electric dipole source pointing in the x-direction is positioned 10 km above the surface. The reason is to produce an approximately plane wave in the vicinity of the scatterer. This source does not produce a true plane wave but is the best approximation made possible with NLAYER. This source setup fits the micropulstion and Schuman resonance but will not be correct to simulate the man made sources correctly since these sources are submerged. See figure 16 for illustration of source position, scatterer position and the environment.

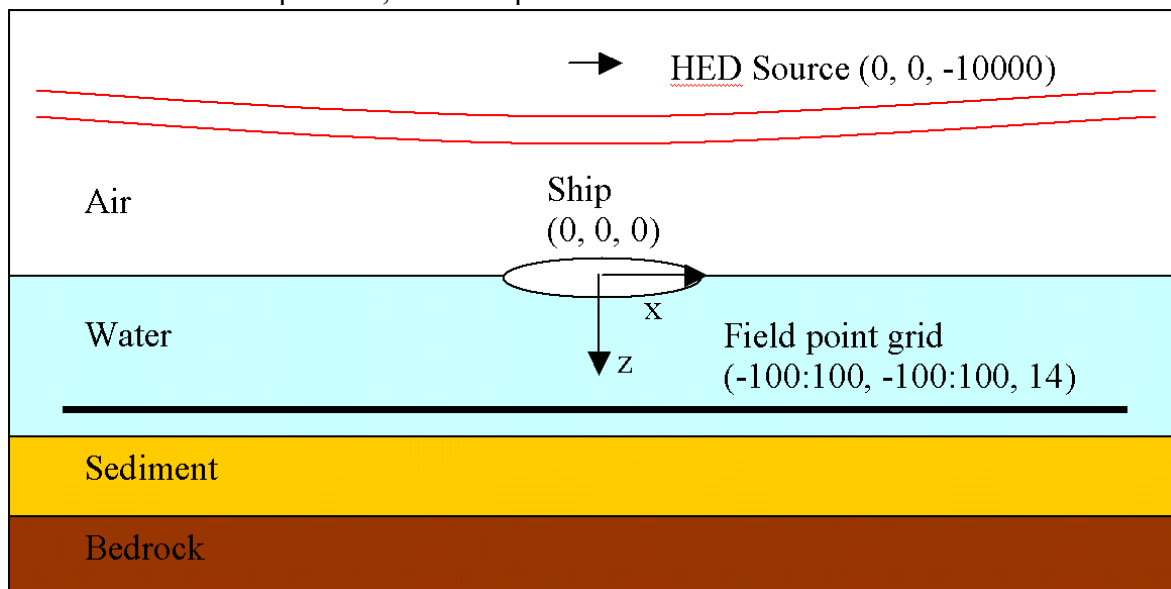


Figure 16. Source, scatterer and field point grid positions in the four layer environment.

The scattered fields are computed for five different frequencies 0.01 Hz, 1 Hz, 10 Hz, 50 Hz and 150 Hz. The first two frequencies correspond to signals similar to micropulsations, the third frequency to Schuman resonances and the last two frequencies to man made signals.

As a scattering object three ellipsoids are used to resemble ships. The dimensions of the scatterers are described in table 3. The ellipsoids are put in the interface between the air and

the water layer so that half of the scatterer is submerged. The stratified environment consists of four layers, air, water, sediment, and bedrock and is described in the table 4. The ship is positioned in the origin and is said to be heading  $0^\circ$  in the x-direction.

Scattering object nr	1	2	3
Ellipsoid x-radii	25 m	7.5 m	2.5 m
Ellipsoid y-radii	5 m	2 m	1 m
Ellipsoid z-radii	5 m	2 m	1 m

Table 3. Shape of scattering object.

	Layer thickness	Conductivity $\sigma$ [S/m]	Permittivity $\epsilon_r$
Air	-	0	1
Water	15	0.800	81
Sediment	10	0.040	81
Bedrock	-	0.001	1

Table 4. Layer data for shield effect simulation.

Two different sets of calculations are done. The first set is to investigate how the scattered fields change when the heading of the ship is altered and the second set is to compare the effects for the three different scattering objects. In both sets the scattered fields are computed for field points one meter over the sediment layer.

The fields are computed at a grid around the scattering object and compared to the fields from the source when the scattering object is absent. Directly beneath the ship the scattered field is in anti phase with the incoming field and will create a minimum, and around the scatterer two local maxima occur. When the ship is rotated from being parallel to the dipole the intensity of the scattered field decreases as can be seen in figure 17. The two local maxima move when the scatterer is rotated in the xy-plane, so that the maxima coincide with points close to the maximum and minimum x-coordinate of the scatterer. The result of this is that the maxima move closer together when the scatterer is turned from  $0^\circ$  to  $90^\circ$ . For the same reason the local maxima will be almost  $45^\circ$  from the origin when the scatterer is turned  $45^\circ$  see figure 18a-c.

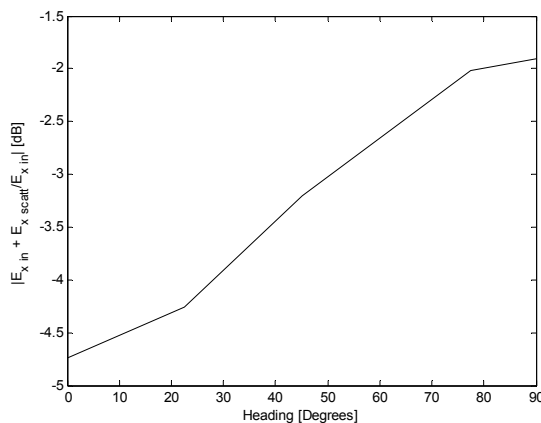


Figure 17. Relative field intensity as a function of heading.

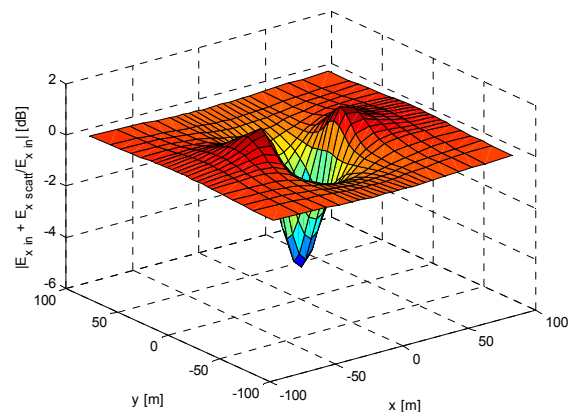


Figure 18a. Relative field intensity when the scatterer is heading in the  $0^\circ$  direction.

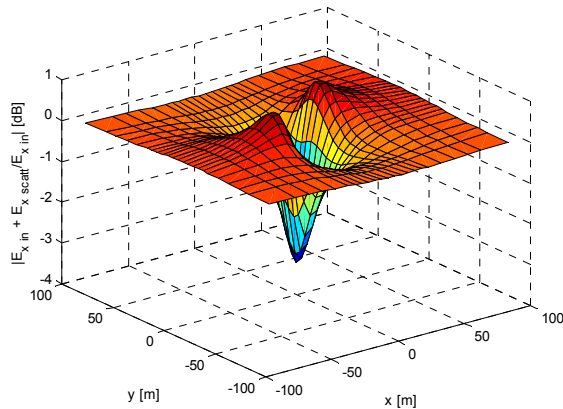


Figure 18b. Relative field intensity when the scatterer is heading in the  $45^\circ$  direction.

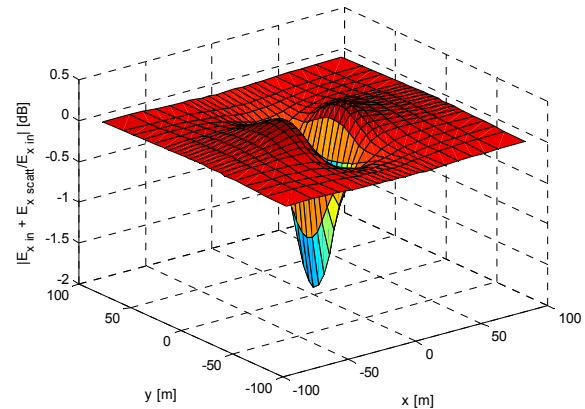


Figure 18c. Relative field intensity when the scatterer is heading in the  $90^\circ$  direction.

In the previous examples scattering object nr: 1 was used and the frequency was 10 Hz. As can be seen in figure 17 the change in the background when the ship is parallel to the dipole is  $-4.7$  dB. This deviation is measurable. The same calculations are made for the four other frequencies, see figure 19. The deviation in the background increases slightly for lower frequencies and it is almost unchanged for higher frequencies. For both scattering objects, nr: 2 and nr: 3, the deviation in the background is small and would be very difficult to measure, figure 20 & 21, and the deviation varies with the frequency in the same manner as for the larger scatterer. The present available equipment needs a deviation of at least one or two dB from the background to detect a passing ship in this environment. These simulations make it evident that a small boat approximately 5 m long will not produce a detectable deviation in the background but a larger ship would.

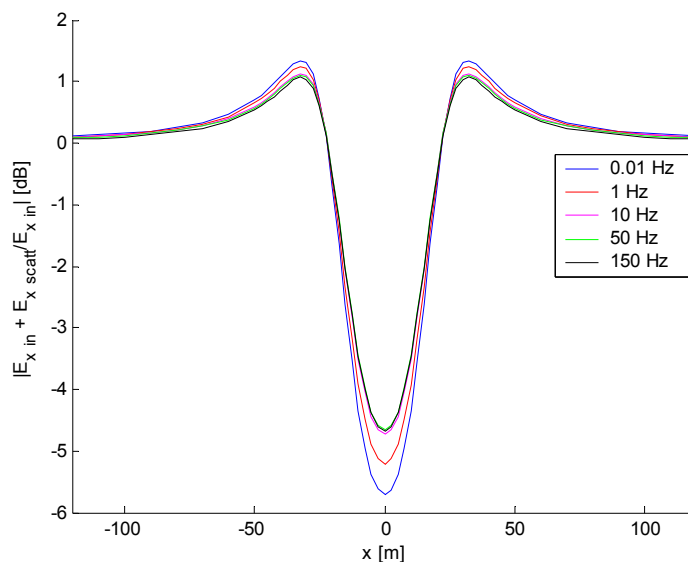


Figure 19. Relative field intensity for scattering object nr: 1. ( $y = 0$  m heading  $0^\circ$ )

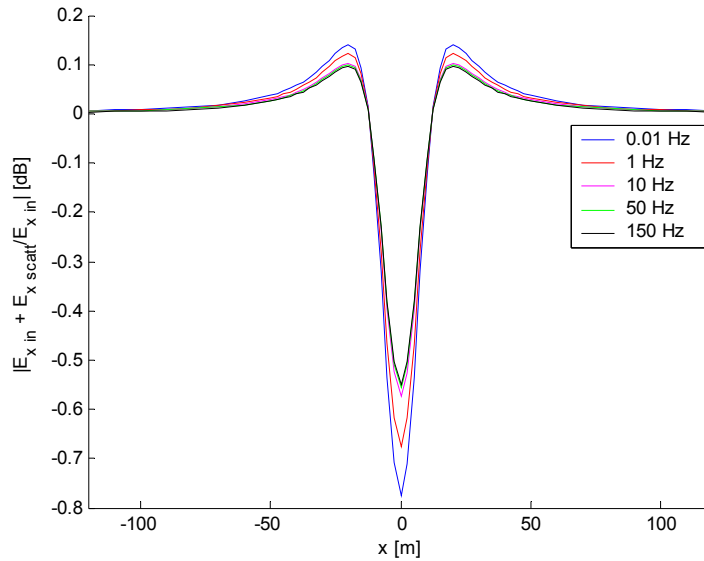


Figure 20. Relative field intensity for scattering object nr: 2. ( $y=0$  m heading  $0^\circ$ )

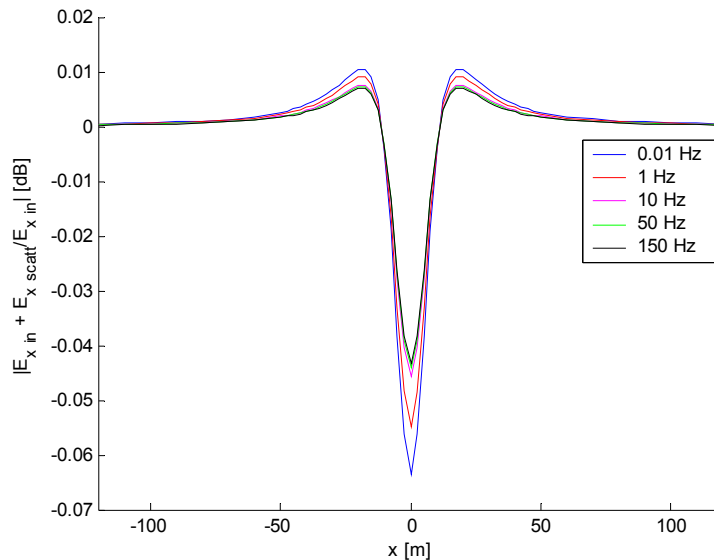


Figure 21. Relative field intensity for scattering object nr: 3. ( $y=0$  m heading  $0^\circ$ )

The calculations performed in this example are close to the limitations of the program. EMSCATT uses NLAYER to compute the Dyadic Green's functions and when parts of the scattering object is positioned in the air it will cause numerical convergence problems for NLAYER when the frequency is very low and the source and the field points are close to the layer interface between air and water. This prevents the use of finer meshes for small scatterers in the surface layer interface at frequencies around 0.01 Hz or improved accuracy in the numerical integration over a face. To prevent some problems the nodes at the boundary in the mesh is moved  $10^{-12}$  m under the layer interface in to the water layer, without this modification there wouldn't be possible to compute the scattering from the 5 m long ellipsoid.

## **Conclusions**

A program computing scattering from perfectly conducting objects situated in multiple layers have been developed and the theory and results are presented in this report. The environment is a horizontally stratified medium and the scattering object is an ellipsoid or a super-ellipsoid. The method used to compute the current density on the scattering objects surface is a boundary element method.

Modifications of the mesh used in the BEM code have to be made when the scatterer is positioned in more than one layer. The method to modify the mesh divides the faces in the mesh so no face is positioned in more than one layer. The problems with this method is presented and discussed and a method how to remove unwanted faces in the mesh is presented. An alternative method of mesh refinement is also suggested.

The convergence of the solution is compared with a well documented program NLAYSCA, and found to converge very well for meshes consisting of 128 faces or more. To decrease computation time an approximation of the Dyadic Green's function in a face is made which reduces the computation by a factor of six. It is shown in this report that there is a small difference between the results achieved with the approximation and without it. The computation time gained could instead be used to increase mesh resolution.

Since there is no other program or measured data of scattering from an object positioned in more than one layer when this report was written, two numerical examples were created to illustrate the use of the program and its limitations.

The first numerical example is a large scattering object positioned in a water sediment boundary with a moving source that passes the scatterer at close range. This example illustrates the importance of mesh refinement when the source is close to the scatterer.

The second example is to investigate the scattered fields from a surface vessel caused by the electric background field. The ships are modeled as a perfectly conducting cigar shaped object which is positioned in the air-water boundary. From the results it is deduced that for large ships it is possible to detect a significant deviation in the background caused by the scattered fields.

## **Acknowledgement**

The supervisors of this work were Johan Mattsson and Peter Krylstedt. I am very grateful for their support and advice during this work. I also want to thank Leif Abrahamsson for always having time to answer my questions regarding NLAYER.

## References

- [1] J. Mattsson, A computer program for EM-scattering by smooth 3D-objects in horizontally stratified media, Scientific report FOA-R--99-01092-409--SE, ISSN 1104-9154, March 1999.
- [2] J. Mattsson, EMS-BEM An electromagnetic ELF scattering program, Internal series FOA Dept of Passive Sonar, Magnetism and Seismology, FOA-R--99-00427-409--SE, February 1999.
- [3] L. Abrahamsson and B. L. Andersson, N-LAYER – An ELFE code for horizontally stratified media, Technical report FOA-R--97-00586-409-SE, ISSN 1104-9154, October 1997.
- [4] Y. Saad and M. H. Schultz, GMRES: A generalized minimal residual algorithm for solving nonsymmetric linear systems, SIAM J. Sci. Stat. Comput. 7 (1986), no. 3, 856-869.
- [5] C. T. Tai, Dyadic Green Functions in Electromagnetic Theory, 2<sup>nd</sup> ed., IEEE PRESS, New-York, 1993
- [6] K. E. Atkinson, User's guide to a boundary element package for solving integral equations on piecewise smooth surfaces, Tech. report 1994, Dept. of Mathematics, University of Iowa, 1994.
- [7] J. Mattsson, Modelling of electromagnetic ELF scattering by smooth 3D objects submerged in water, Scientific report FOA-R--97-00519-409--SE, ISSN 1104-9154, June 1997.
- [8] S. Ström, Introduction to integral representations and integral equations for time harmonic acoustic, Electromagnetic and elastodynamic wave fields, North-Holland, Amsterdam, 1991
- [9] A.P. Nickolaenko and M. Hayakawa, Resonance in the earth-ionosphere cavity, Kluwer Academic Publishers, Dordrecht, 2002.